IFSCC 2025 full paper (IFSCC2025-621)

A Unique Silk Microneedle Delivery Platform Integrated with Co-Delivery Nanoliposomes Facilitates Efficient and Safe Skin Pigmentation Treatment

Siyuan Chen[1, 2*], Dan Luo[1], Dan Chen[1], Rui Liu[1], Jun Deng[2], Wei Liu[2*]

[1] Hangzhou Rebtech/Wuhan Best-Carrier Nanomedicine Research Institute, China;

[2] National Engineering Research Center for Nanomedicine, Huazhong University of Science and Technology, Wuhan, China

Email: maggie@hzrebtech.com, siyuan.chen@njtech.edu.cn

Abstract

The skin pigmentation greatly affects the skin appearance. A variety of whitening active ingredients suffer from low bioavailability, low effectiveness and side effects. The majority of whitening skincare products cannot efficiently penetrate the stratum corneum to reach to the basal layer where the melanocytes exist. Moreover, these products usually only have one single whitening target, and thus considerably hampers their functionality. Besides, the skin irritation and instability problem further limit their application. Therefore, new technology is urgently needed for effective skin pigmentation treatment without causing adverse effects.

Herein, we developed a microneedle (MN) delivery platform integrated with co-delivery nanoliposomes (NLPs) for effective and safe skin pigmentation treatment. Glabridin decreases melanogenesis through suppression of PKA/MITF and MAPK/MITF signaling pathways. Nicotinamide inhibits melanin transfer from melanocytes to keratinocytes. Nonapeptide-1 impedes the action of MSH and hinders the activation of tyrosinase. By scientifically combining these three ingredients targeting different pathways, a synergistic effect could be achieved for pigmentation treatment. NLPs encapsulation can remarkably enhance the stability, improve the bioavailability and release payloads in a sustained and controlled way. By further incorporating the co-delivery NLPs into a silk fibroin/HA-based biodegradable MN delivery platform, superior effectiveness could be achieved by efficient skin penetration.

The co-delivery NLPs incorporated MN displayed a sharp pyramidal needle shape. Similar to the NLPs without MN incorporation, the NLPs released from MN also effectively enhanced the cellular uptake, decreased tyrosinase activity, and inhibited the expression of TYR mRNA and TRP-1 mRNA which are related to melanin synthesis. In vitro skin penetration results showed that compared to the NLPs without MN facilitation, the NLPs incorporated MN penetrated deeper and delivered cargo to the basal layer of skin. The 3D whitening skin model also showed decreased melanin content and decreased L* value after MN treatment. No skin irritation was observed after MN administration in the patch test, indicating great safety. This co-delivery NLPs incorporated MN delivery platform with unique effectiveness and safety shed light on the development of new technology for skin pigmentation treatment.

---

1. Introduction

Skin pigmentation disorders, characterized by hyperpigmented patches or spots, significantly impact aesthetic appearance and psychological well-being [1]. The pathogenesis of pigmentation involves complex mechanisms, primarily driven by melanocyte hyperactivity and dysregulated melanogenesis [2]. Key pathways include the activation of tyrosinase—the rate-limiting enzyme in melanin synthesis—and upstream signaling cascades such as the protein

kinase A (PKA)/microphthalmia-associated transcription factor (MITF) and mitogen-activated protein kinase (MAPK)/MITF pathways, which regulate melanocyte proliferation and pigment production [3]. External factors like UV exposure and hormonal changes further exacerbate melanin overproduction, leading to conditions such as melasma and post-inflammatory hyperpigmentation [4].

Current therapeutic strategies for pigmentation include topical agents (e.g., hydroquinone, retinoids, and kojic acid), chemical peels, and laser therapies [5,6]. While these modalities aim to inhibit tyrosinase activity, reduce melanosome transfer, or accelerate epidermal turnover, they face critical limitations. Topical agents often exhibit poor bioavailability due to the impermeable stratum corneum barrier, with less than 5% of applied doses penetrating the skin's basal layer where melanocytes reside. Furthermore, many compounds, such as hydroquinone, pose risks of skin irritation, erythema, and long-term toxicity[7]. Monotherapy approaches targeting a single pathway also fail to address the multifactorial nature of melanogenesis, resulting in suboptimal efficacy [8].

To overcome these challenges, nanotechnology-based drug delivery systems have emerged as promising tools [9]. Nanoliposomes (NLPs), for instance, enhance drug stability, prolong release kinetics, and improve epidermal permeation by fusing with lipid bilayers in the stratum corneum[10]. Studies demonstrate that NLPs encapsulating antioxidants like vitamin C or resveratrol significantly reduce oxidative stress and melanin synthesis in vitro and in vivo [11,12]. Our research group has successfully developed several NLP-based delivery systems that enhance transdermal delivery efficiency. For instance, we co-encapsulated copper peptide, acetyl tetrapeptide-3, and myridamoyl five-peptide-4 into NLPs. This approach not only improved the stability of the active peptides but also achieved a multi-target synergistic effect through the combination of multiple bioactive peptides. Moreover, it enhanced transdermal delivery efficiency and promoted hair growth [13]. Additionally, we developed NLPs loaded with various bioactive peptides. The results showed that NLPs can significantly enhance the drug uptake of relevant target cells [14]. The NLPs encapsulating cationic phenethyl resorcinol developed by our group exhibited a slow-release profile, with significantly improved skin retention and remarkably enhanced transdermal permeability [15]. These outstanding properties of NLPs indicate their suitability for the transdermal delivery.

However, even advanced nanocarriers struggle to achieve sufficient intradermal delivery without auxiliary penetration-enhancing technologies [16]. Microneedles (MNs), minimally invasive devices that create transient microchannels in the skin, have revolutionized transdermal drug delivery [17,18]. Dissolvable MNs composed of biocompatible materials, e.g., silk fibroin (SF) and hyaluronic acid (HA), enable controlled release of payloads directly into the epidermis and dermis, bypassing the stratum corneum barrier [19,20]. Recent innovations, such as Iontophoresis-driven MN platforms, further enhance drug delivery precision and depth, as evidenced by clinical trials showing improved drug permeation and reduced treatment durations [21]. When combined with nanocarriers, MNs synergistically enhance the bioavailability of multi-target therapies, addressing the limitations of conventional approaches [22].

In this study, we developed a biodegradable MN platform integrated with co-delivery NLPs for synergistic pigmentation treatment (Figure 1). The NLPs co-encapsulate three active ingredients: glabridin (a licorice-derived compound suppressing PKA/MAPK-MITF pathways), nicotinamide (inhibiting melanosome transfer), and nonapeptide-1 (blocking α-MSH-induced tyrosinase activation). By targeting multiple melanogenic pathways, this system overcomes the inefficacy of single-mechanism therapies. The silk fibroin/sericin MN matrix ensures sustained release, while NLPs enhance ingredient stability and cutaneous absorption. Preclinical evaluations demonstrate superior depigmenting efficacy and minimal irritation, highlighting the potential of this combinatorial approach to redefine precision dermatology.

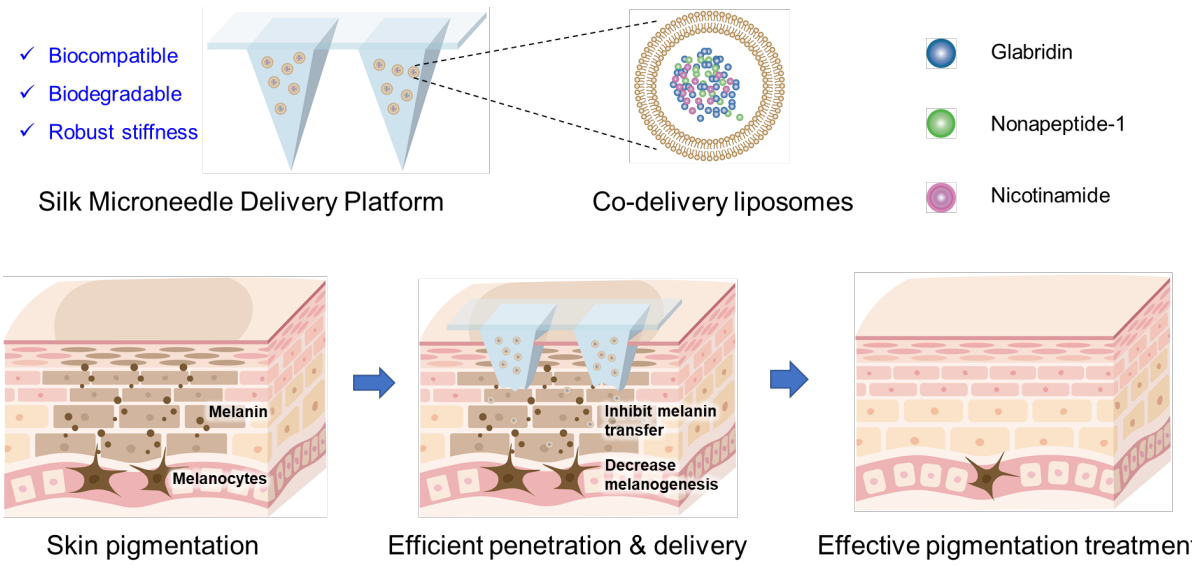

Figure 1. Schematic of a silk microneedle delivery platform integrated with co-delivery nanoliposomes facilitates efficient and safe skin pigmentation treatment.

2. Materials and Methods

2.1 Materials

Glabridin was purchased from Xinjiang Longhuiyuan Pharmaceutical Co., Ltd. Nicotinamide was sourced from LONZA. Nonapeptide-1 were obtained from Nanjing Leon Biotechnology Co., Ltd. Hyaluronic acid (HA, Mw 47 kDa) was purchased from Huaxi Biotechnology Co., Ltd. (Shandong, China). Hydrogenated soy phosphor lipid (99.5%) was purchased from Shanghai Maclean Biochemical Technology Co., Ltd. (Shanghai, China). Rhodamine B and cholesterol were obtained from Aladdin Reagent Co., Ltd. (Shanghai, China). DMEM high-glucose medium, fetal bovine serum, penicillin-streptomycin, trypsin-EDTA were sourced from Gibco, USA. L-DOPA, tyrosine, TritonX-100, and α-Melanocyte Stimulating Hormone (α-MSH) were obtained from Sigma-Aldrich, USA. BCA Protein Assay Kit were purchased from Beyotime Biotechnology, Shanghai. Glycerol were purchased from Sinopharm Group Chemical Reagent Co., Ltd. Silk cocoons were purchased from Jiangsu University of Science and Technology (Jiangsu, China).

2.2 Preparation of NLPs

The co-delivery NLPs were prepared by high-pressure homogenization technology. A 20% (w/w) butanediol water solution containing 8% (w/w) lecithin, 0.2% (w/w) cholesterol, and glabridin was prepared and designated as phase A. In the meanwhile, nicotinamide and nonapeptide-1 were dissolved in distilled water containing 15% (w/w) glycerol to produce phase B. After heating the two phases separately to 45 °C, phase B was added to phase A with mixing, followed by homogenization at 800 bar for 2 times. The unencapsulated ingredients were removed by ultracentrifugation at 15,000 × g for 30 min using an ultrafiltration tube (MWCO 100 kDa, Amicon Ultra, Millipore, Billerica, MA, USA) to obtain the NLPs.

2.3 Characterization of NLPs

The zeta potential, PDI as well as the particle size of the co-delivery NLPs were determined using a Zetasizer/Nano-ZS90 instrument (Malvern Instruments, Malvern, UK) at 25 °C with ultra-pure water as a dispersing medium. The morphology of the co-delivery NLPs was observed by TEM (HT7700, Hitachi, Tokyo, Japan). The content of encapsulated ingredients was determined by high-performance liquid chromatography (HPLC). Ultrafiltration centrifugation was applied to remove the unencapsulated ingredient, and the EE and DL of the co-delivery NLPs were calculated.

2.4 Silk fibroin extraction

SF was extracted from silkworm cocoons according to previous report. The silk cocoons were boiled in 20 mM Na_2CO_3 aqueous solution for 1 h to remove the sericin protein from the cocoons, then rinsed with deionized water for more than six times. After drying in the fume hood for overnight, the SF was dissolved with 9.3 M LiBr solution at 60 °C for 4 h until totally dissolved. The obtained SF solution was dialysis against deionized water using a dialysis bag with MWCO of 3.5 kD_a for 2–3 days. Afterwards, centrifugation (Rcf 17,000 g, 30 min) was utilized for further purification. The final concentration of SF solution was measured by drying a certain volume of SF in the oven and recording the weight. If necessary, the SF solution was concentrated by dialysis against 20 wt% polyethene glycol (PEG Mw 10kDa) until the SF concentration reached to 10 wt%.

2.5 Co-delivery NLPs@MNs fabrication

SF MNs containing co-delivery NLPs were fabrication by micromolding technology. SF solution (10 wt% SF in deionized water) was blended with co-delivery NLPs at SF: NLPs = 7:3 (v/v) ratio.100 μL blended SF solutions were added to PDMS mold ordered from Taizhou Microchip Pharmaceutical Technology Co., Ltd. (10 × 10 array, needle length 600 μm, pitch-to-pitch size tip 600 μm, base size 300 × 300 μm). After centrifugation at 2,100 g for 5 min to fill the tip site, the residue solution was removed. The PDMS mold was air dried for 1 h, and this process was repeated three times to ensure that the MNs tips were filled. 20% (w/v) HA solution was added to the PDMS mold to form the MNs base layer. After air dried for 24 h, the co-delivery NLPs@MNs were carefully demolded from the PDMS mold. The morphology of MNs was characterized by optical microscopy (TE2000, Nikon, Japan) and scanning electron microscope (SEM, JSM-IT200, JEOL Japan Electronics Co., Ltd, Japan).

2.6 MNs mechanical properties characterization

The mechanical strength of fabricated MNs was characterized by a mechanical axial compressive test. The MNs were placed on a stainless- steel base plate in a texture analyzer (MAX-1KN–H, JISC Co., Ltd., Japan). An axial force was applied vertically to the axis of the array at a constant speed of 6 mm/min. When the moving sensor touched the uppermost point of the needles, the force measurement was started. The probe pressure and displacement were recorded by the analyzer until the sample was entirely deformed.

In vitro skin insertion was performed using porcine skin (provided by Qinglongshan Animal Breeding Plant in Jiangsu, China). Prior to the puncture experiment, the porcine skin was cut into 3 × 3 cm square shape, and the MNs were pressed on the skin with 50 N force for 1 min. After removing the MNs, the skin was stained with trypan blue for 5 min, and then the residual dye was removed by tissue. The inserted pinholes were observed by an optical microscope.

2.7 In vitro skin permeation

In vitro permeability was evaluated via Franz diffusion cells. Porcine skin samples were secured between the donor and receptor chambers, with 0.5 mL of RhoB-loaded NLPs or free RhoB solution applied topically to the skin surface. For the MN-treated group, RhoB-NLPs@MNs were applied to the skin for 1 minute and secured with adhesive tape, ensuring equivalent RhoB content across all groups. The receptor chamber was filled with 7 mL of medium (saline containing 20% w/w 1,2-propanediol), and permeation studies were conducted at 32°C under continuous magnetic stirring (300 rpm). After 2 and 4 h administration, skin samples from each group were collected, rinsed with saline, and embedded in optimal cutting temperature (OCT) compound. Sections of 10 μm thickness were prepared using a cryostat (CryoStar NX50, Thermo Scientific, Shanghai, China). RhoB transdermal distribution was analyzed via confocal laser scanning microscopy (CLSM, FV3000, Olympus, Tokyo, Japan) with excitation/emission wavelengths set to 546 nm and 568 nm, respectively.

2.8 Cell culture

Mouse melanoma cells (B16F10) were cultured in DMEM medium supplemented with 10% fetal bovine serum and 1% penicillin/streptomycin. All cells were trypsinized using trypsin-EDTA and cultured in a humidified incubator containing 5% carbon dioxide at 37°C.

2.9 In vitro cytotoxicity

1×10^4 cells were incubated in 96-well plates (Corning, New York, NY, USA) overnight, respectively, and then treated with various samples for 24 h. The cells treated with DMEM only served as the control group. After 24 h incubation, each well was washed with PBS and treated with 100 μL 0.5 mg/mL MTT solution. After incubation for 4 hours, the MTT solution was removed and 100 μL DMSO solution was added. The absorbance at 562 nm was collected.

2.10 Cellular uptake

The cellular uptake of RhoB-Lip by B16F10 cells was observed by confocal laser microscopy. B16F10 cells were inoculated with 2×10^5 cells per well in a 20 mm glass-bottom culture dish for 24 h. After 24 h, the culture medium was removed, washed three times with PBS, and the cells were treated with free RhoB solution or RhoB-Lip with the same RhoB concentration for 2 h. After rinsing with PBS for three times, 10 μg/mL Hoechst was added for nuclear staining. After the staining for 30 min, the dye was removed, and the cells were washed three times with PBS, and imaged using a laser scanning confocal microscope (LSM700, ZEISS, Germany).

2.11 Cellular skin-brightening study

B16F10 cells were seeded in 6-well plates at a density of 2×10^5 cells per well and cultured for 24 h. Next, these cells were treated with 100 nmol/L α-MSH along with the free ingredients or co-delivery NLPs@MNs with the same ingredients concentration. B16F10 cells treated with DMEM only served as the control group, and B16F10 cells treated with 100 nM α-MSH only served as the model group. After 48 h culture, the culture medium was discarded, and triton X-100 was added to each well . The 6-well plates were frozen at −80°C for 30 min, then thawed at room temperature and centrifuged. A sample of 100 μL of supernatant was withdrawn and transferred to a 96-well plate. A sample of 100 μL 0.1% w/v% L-dopa solution was added to each well and the reaction was carried out at 37°C for 2 h. The absorbance of each well was measured by the microplate reader. The relative content of melanin was determined by sodium hydroxide lysis. B16F10 cells were seeded in a 12-well plate at a density of 1×10^5 cells per well and cultured for 24 h, and then were treated in the same grouping and method as above. After 48 h culture, the culture medium was discarded and replaced with 500 μL 1 mol/L sodium hydroxide solution containing 10% DMSO. After incubation at 60 °C for 4 h, the plates were centrifuged, and 100 μL of supernatant was withdrawn from each well and transferred to a 96-well plate. The absorbance of each well was measured by the microplate reader at 495 nm wavelength. The relative melanin production was calculated.

2.12 3D skin model skin brightening study

A UVB-stimulated 3D melanin model (MelaKutis®, Guangdong Boxi Biotechnology Co., Guangzhou, China) was used to construct an in vitro skin damage model. The brightening efficacy was evaluated by measuring the three dimensions of apparent chromaticity, apparent luminance (L* value) and melanin content of the skin model. The 3D melanin model was inoculated in 6-well plates. The kojic acid group, free ingredients group and co-delivery NLPs@MNs group were treated with kojic acid, free ingredients or co-delivery NLPs@MNs with the same concentration as the free ingredients, respectively. In this experiment, surface administration was performed in a gentle circular manner on the third and fifth day, respectively. The model group, the kojic acid group, the free ingredients group and co-delivery NLPs@MNs group were treated with UVB irradiation daily, while the control group was not irradiated with UVB and only the culture solution was changed daily. The apparent colorimetric evaluation was performed by a camera.

2.13 Statistical analysis

All data points were replicated three times (n = 3). Results and graphical data are reported as means with 95% confidence intervals for standard deviations. Statistical significance of differences was assessed using Student ’s t-test. $p < 0.05$ was considered a statistically significant difference.

3. Results

3.1. Particle size and stability

The formulated co-delivery NLPs demonstrated a mean particle size of 146.13 ± 0.55 nm and a polydispersity index (PDI) of 0.16 ± 0.04 (Figure 1a). Transmission electron microscopy (TEM) analysis revealed that the co-delivery NLPs maintained a homogeneous spherical morphology. These dimensions aligned closely with the hydrodynamic size measurements obtained from dynamic light scattering (DLS). Following one month of low-temperature storage (4°C), the co-delivery NLPs exhibited negligible variation in particle size (Figure 1b). Furthermore, the formulations retained their transparency without signs of delamination or phase separation, demonstrating their favorable storage stability.

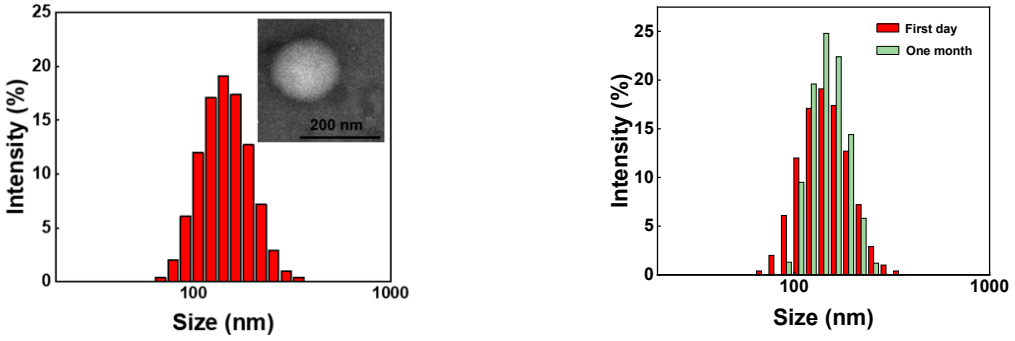

(**a**) (**b**)

Figure 1. Characterization of co-delivery NLPs (a) The particle size distribution and TEM image of the co-delivery NLPs.(b) The particle size distribution change of co-delivery NLPs after one month.

3.2. Morphological characterization of MNs MNs

SF MNs integrated with co-delivery NLPs were manufactured via micromolding using 10 × 10 array PDMS molds. The co-delivery NLPs-incorporated SF MNs exhibited well-defined pyramidal needle structures (Figure 2a), with a height of approximately 600 μm—sufficient to penetrate the stratum corneum and target the epidermis. SEM analysis further confirmed the morphological characteristics of the MNs. As illustrated in Figure 2b, the NLPs-integrated SF MNs retained a sharp-tipped geometry and surface smoothness comparable to pristine SF MNs, demonstrating that the inclusion of co-delivery NLPs did not compromise needle integrity or fabrication quality.

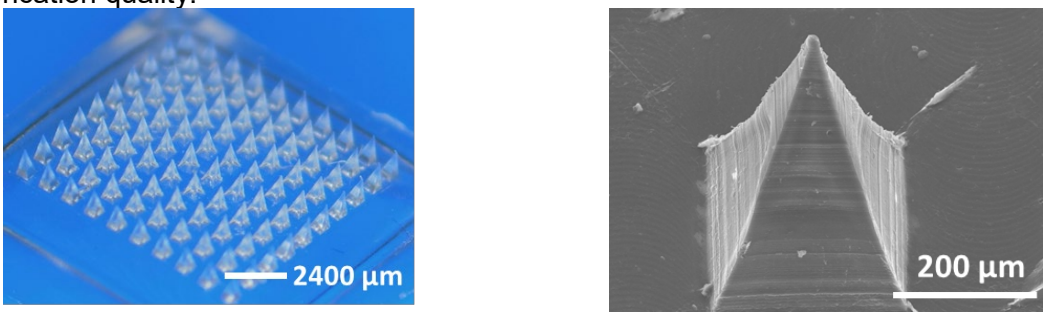

(**a**) (**b**)

Figure 2. Morphology of co-delivery NLPs@MNs characterized by (a) optical microscopy; (b) SEM.

3.3. The mechanical properties of MNs

The mechanical strength of SF-based MNs incorporating co-delivery NLPs was evaluated using a texture analyzer. To achieve the minimum force required for skin insertion (0.058 N/needle), mechanically robust and biocompatible SF was combined with co-delivery NLPs during MN fabrication to improve structural integrity. As shown in Figure 3a, the absence of a fracture point in the co-delivery NLPs@MNs suggests that the needles underwent bending deformation rather than fracture during testing—a behavior typical of polymeric MNs. Pure SF MNs exhibited a steeper force-displacement curve slope compared to co-delivery NLPs@MNs, confirming that SF enhances mechanical strength. This property arises from the heavy chain of SF, which contains 11 highly repetitive crystalline domains, imparting exceptional rigidity.

For in vitro skin penetration studies on porcine tissue, trypan blue staining revealed visibly distinct micropores post-administration (Figure 3b), confirming that the MNs successfully generated microchannels to facilitate efficient transdermal delivery. Collectively, these findings demonstrate that while NLPs integration reduces mechanical strength, the co-delivery NLPs@MNs retained sufficient rigidity to breach the skin barrier and access the upper epidermal or dermal layers.

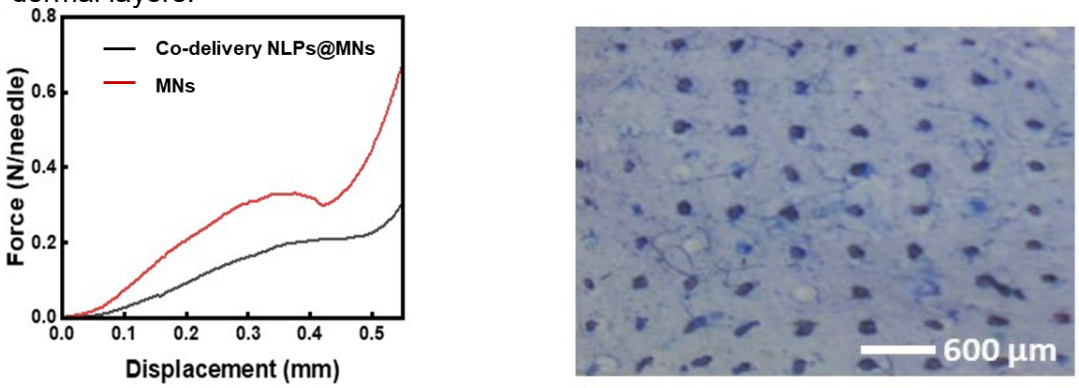

(**a**) (**b**)

Figure 3. (a) Mechanical strength of MNs fabricated by various materials tested by a texture analyzer. (b) Trypan blue staining showing the formation of microchannels after treatment with co-delivery NLPs@MNs.

3.4. In vitro skin permeation

Limited skin permeation is a key factor contributing to the low therapeutic efficacy of transdermal drug delivery. Microneedles (MNs) effectively enhanced the transdermal delivery of co-delivery NLPs by bypassing the stratum corneum (SC) barrier. The permeation behavior of co-delivery NLPs@MNs was evaluated using isolated porcine skin. Rhodamine B (RhoB), employed as a fluorescent tracer, was encapsulated within NLPs. Compared to free RhoB solution and RhoB-loaded NLPs (RhoB-NLPs), RhoB-NLPs@MNs demonstrated significantly stronger red fluorescence intensity and deeper penetration depth in treated skin (Figure 4). These results indicate that the MN-based delivery platform markedly improved both transdermal penetration and permeation depth of RhoB. This improvement can be attributed to the MN-mediated disruption of the SC barrier, enabling efficient delivery of encapsulated therapeutics to targeted tissue layers.

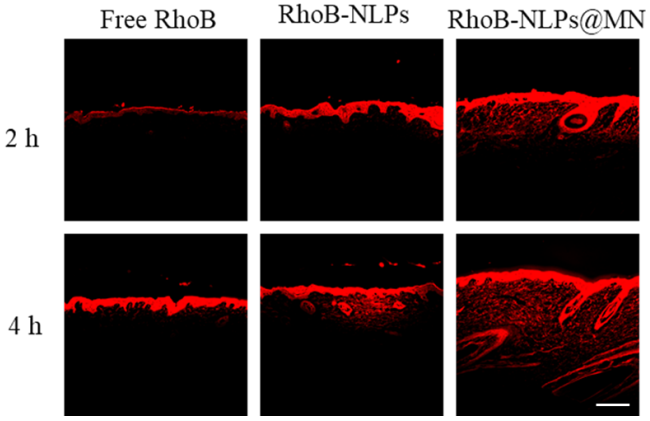

Figure 4. In vitro skin penetration. Confocal microscope images showing transdermal delivery process for treating skin with various sample for 4 h. Scale bar: 200 μm.

3.5. In vitro cytotoxicity

The in vitro cytotoxicity of blank NLPs, co-delivery NLPs, and co-delivery NLPs@MNs was evaluated via the MTT assay. As depicted in Figure 5a, within the lipid concentration range of 0.1 - 2500 μg/mL, the survival rates of B16F10 cells treated with blank NLPs and co-delivery

NLPs at various lipid concentrations all exceeded 80%. This finding suggests that the cytotoxicity of both blank NLPs and co-delivery NLPs was negligible across a broad lipid concentration range. Figure 5b illustrates the cytotoxicity of co-delivery NLPs and co-delivery NLPs@MNs on B16F10 cells at the same encapsulated ingredient concentration. Evidently, neither group exhibited cytotoxicity when the ingredient concentration ranged from 0.1 to 20 μg/mL. These data demonstrate that co-delivery NLPs and co-delivery NLPs@MNs demonstrate a high level of cellular safety, with minimal toxicity to B16F10 cells across a wide range of lipid and ingredient concentrations.

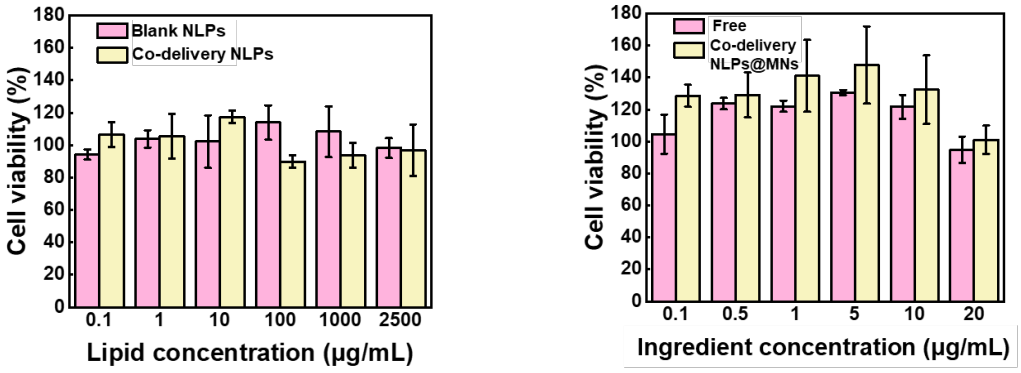

Figure 5. In vitro cytotoxicity. (a) In vitro cytotoxicity of the blank NLPs and co-delivery NLPs against B16F10 cells with the same lipid concentration. (b) In vitro cytotoxicity of free ingredients and co-delivery NLPs@MNs against B16F10 cells with the same ingredient concentration.

3.6. Cellular uptake

The intracellular delivery of the model payload RhoB to B16F10 cells was assessed using confocal microscopy. As shown in Figure 6, minimal red fluorescence was detected in B16F10 cells incubated with free RhoB solution for 4 hours, suggesting limited cellular internalization of RhoB. In contrast, significantly stronger RhoB-derived fluorescence was observed in cells treated with RhoB-loaded NLPs released from MNs at an equivalent RhoB concentration. These findings demonstrate that NLPs enhance cellular uptake efficiency, and their integration into the MN delivery platform did not compromise their inherent cellular internalization behavior.

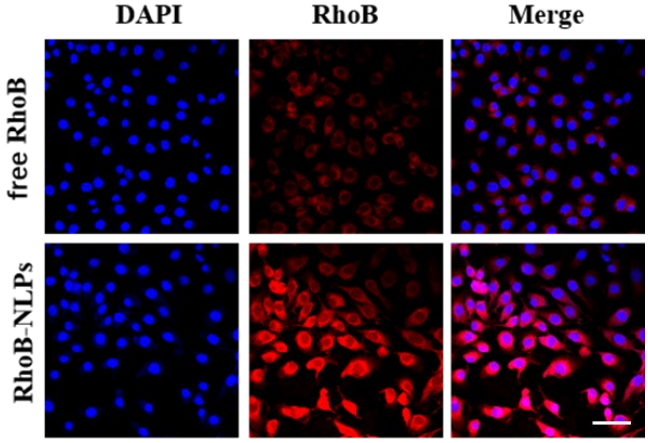

Figure 6. Celluar uptake. Visualization of cellular uptake of RhoB by B16F10s using a CLSM after incubation for 4 h. Scale bar: 50 μm.

3.7 Celluar brightening effect

As shown in Figure 7a, when compared with the model group, the production of tyrosinase in B16F10 cells was significantly decreased in both the free ingredients group and the co-delivery NLPs@MNs group ($p < 0.01$). Moreover, in contrast to the free ingredients group, the tyrosinase inhibition rates of B16F10 cells were notably elevated in the co-delivery

NLPs@MNs group at concentrations of 5.0 mg/L and 10.0 mg/L ($p < 0.01$ and $p < 0.05$, respectively). This finding implies that encapsulation within the nanocarrier can effectively reduce tyrosinase activity, and the incorporation of microneedles (MNs) does not impair the functionality of nanoliposomes (NLPs).

Figure 7b presents the inhibitory effect of free ingredients and co-delivery NLPs@MNs on melanogenesis in B16F10 cells. The elevated melanin content in the model group indicates the successful establishment of a high melanin expression model. In comparison to the model group, melanin production in B16F10 cells was significantly reduced in both the free ingredients group and the co-delivery NLPs@MNs group ($p < 0.01$). More crucially, when compared with the free ingredient group, co-delivery NLPs@MNs significantly decreased melanin production in B16F10 cells at concentrations of 5.0 mg/L and 10.0 mg/L ($p < 0.01$), suggesting that co-delivery NLPs@MNs can efficiently suppress melanogenesis.

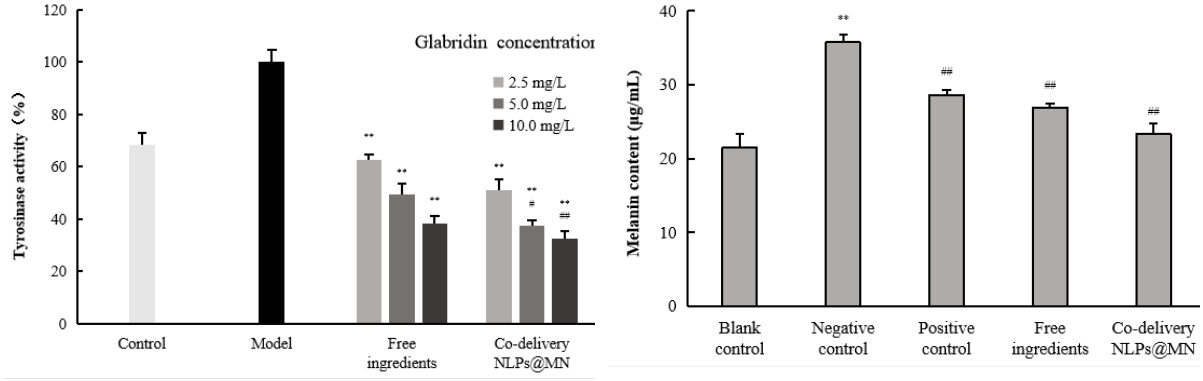

(**a**) (**b**)

Figure 7. Cellular skin-brightening effect. (a) tyrosinase activity and (b) melanin content of B16F10 cells treated with various samples. Compared with model, $^{**}p < 0.01$; compared with free ingredients, $^{\#}p < 0.05$, $^{\#\#}p < 0.01$.

3.8 3D skin-brightening effect

UVB irradiation was applied to the 3D melanin skin model (MelaKutis®) to assess the skin-brightening efficacy of the test samples by analyzing the alterations in apparent chroma and apparent luminance (L* value). On the basis of the 3D melanin skin model, in comparison with the negative control group, the co-delivery NLPs@MNs demonstrated a remarkable whitening effect in terms of apparent chroma (Figure 9a), accompanied by a significant increase in apparent luminance (L* value, Figure 9b). These findings suggest that the co-delivery NLPs@MNs are capable of improving apparent chroma and enhancing apparent luminance, thus exhibiting skin-whitening efficacy. Moreover, its superiority in significance surpasses that of the free ingredients and the VC group (positive control), which implies a more potent whitening effect after nano-encapsulation. Furthermore, MNs incorporation did not affect the functionality of NLPs.

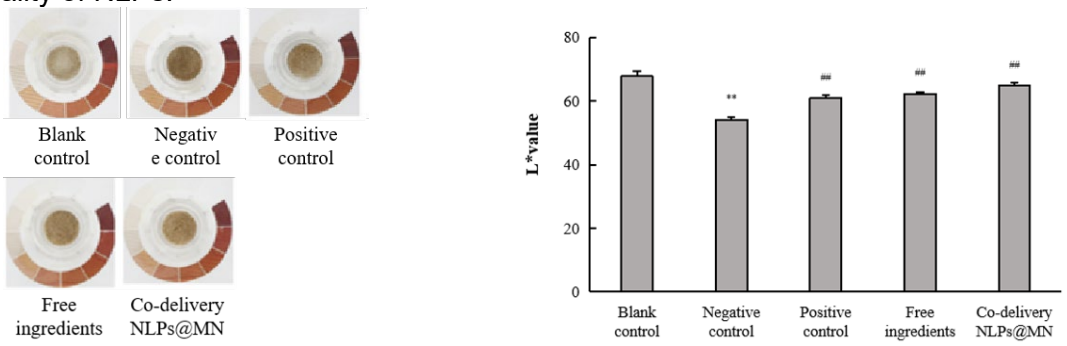

(**a**) (**b**)

Figure 8. 3D skin-brightening effect. (a) Apparent chroma and (b) apparent luminance test results of 3D skin model. Compared with blank control, $^{**}p < 0.01$; compared with negative control, $^{\#\#}p < 0.01$.

4. Conclusion

This study successfully developed a MN platform integrated with co-delivery NLPs for synergistic skin pigmentation treatment. The co-delivery NLPs, encapsulating glabridin, nicotinamide, and nonapeptide-1, showed a small particle size and good storage stability. The co-delivery NLPs @MNs had sufficient mechanical strength to penetrate the skin barrier. In vitro skin permeation studies demonstrated that the co-delivery NLPs @MNs significantly improved transdermal penetration and permeation depth compared to free solution. The in vitro cytotoxicity assays indicates high cellular safety. Cellular uptake experiments showed that NLPs enhanced the internalization of the payload into B16F10 cells, and the MN delivery system did not compromise this behavior. Both in cellular and 3D skin models, co-delivery NLPs@MNs significantly reduced tyrosinase activity and melanin production compared to the model group. Moreover, they outperformed the free ingredients group, suggesting that nano-encapsulation and the MN delivery system synergistically enhanced the skin-whitening efficacy. Overall, this combinatorial approach of co-delivery NLPs@MNs has great potential to redefine precision dermatology for the treatment of skin pigmentation disorders.

References

[1] S.S. Sulaimon, B.E. Kitchell, Vet. Dermatol. 14 (2003) 57–65.
[2] J.Y. Lin, D.E. Fisher, Nature 445 (2007) 843–850.
[3] V. Sobolev, E. Tchepourina, A. Soboleva, E. et al., Cells 14 (2025).
[4] S. Rajanala, M.B. de C. Maymone, N.A. Vashi, Dermatol. Online J. 25 (2019).
[5] I.M. Fabian, E.S. Sinnathamby, C.J. Flanagan, et al., Cureus 15 (2023) e48840.
[6] R.R. Riahi, A.E. Bush, P.R. Cohen, 17 (2016) 265–276.
[7] Z Gu, X Chen, Adv. Drug Deliv. Rev. 127 (2018) 1–2.
[8] C. Li, J. Wang, Y. Wang, et al., Acta Pharm. Sin. B 9 (2019) 1145–1162.
[9] J.F. Coelho, P.C. Ferreira, P. Alves, et al., EPMA J. 1 (2010) 164–209.
[10] S. Martins, B. Sarmento, D.C. Ferreira, et al., Int. J. Nanomedicine 2 (2007) 595–607.
[11] V.P. Torchilin, Nat. Rev. Drug Discov. 4 (2005) 145–160.
[12] V.P. Torchilin, Nat. Rev. Drug Discov. 13 (2014) 813–827.
[13] L.W. Tian, D. Luo, D. Chen, et al., J. Drug Deliv. Sci. Technol. 72 (2022) 103381.
[14] F. Han, D. Luo, W. Qu, et al., J. Drug Deliv. Sci. Technol. 57 (2020) 101693.
[15] T. Wei, D. Chen, H. Mei, et al., Nano Life 10 (2020) 2040009.
[16] W. Liu, B. Hou, D. Ma, et al., J. Drug Deliv. Sci. Technol. 99 (2024) 105953.
[17] S. Yang, Y. Xu, M. Zhu, et al., Adv. Mater. 2411112 (2024) 1–20.
[18] E. Larran˜eta, R.E.M. Lutton, A.D. Woolfson, et al., Mater. Sci. Eng. R Reports 104 (2016) 1–32.
[19] L.K. Vora, A.H. Sabri, Y. Naser, et al., Adv. Drug Deliv. Rev. 201 (2023) 115055.
[20] K. Lee, C.Y. Lee, H. Jung, Biomaterials 32 (2011) 3134–3140.
[21] M. Peng, Z. Heng, D. Ma, ACS Appl. Mater. Interfaces 16 (2024) 70378–70391.
[22] W. Zhang, Shuting; Zhou, Hong; Chen, Xuan; et al., ACS Appl. Mater. Interfaces 16 (2024) 15701–15717.